# Nonlinear fluence dependencies in femtosecond laser ablation of metals and dielectric materials

**Tatiana E. Itina**
**Mikhail Mamatkulov**
**Marc Sentis**
Université de la Méditerranée
Parc Scientifique et Technologique de Luminy
Laboratoire Lasers, Plasmas et Procédés Photoniques
(LP3 UMR 6182 CNRS)
Case 917, 13288 Marseille, France
E-mail: itina@lp3.univ-mrs.fr

**Abstract.** We address the peculiarities of femtosecond laser ablation of both metallic and dielectric materials. The ablation process is investigated using two numerical models. For metals, a hydrodynamic model is used that describes the laser light absorption together with heat and pressure wave propagations and the material motion. This model is used to study laser ablation at different fluences for two metals with different strengths of the electron-ion coupling. In these calculations, the role of the temperature-dependent electron heat conduction is demonstrated. For dielectrics, material ionization and laser light absorption processes are modeled in both one and two dimensions. The saturation of the light absorption, and, hence, of the ablation depth, is shown to take place in dielectric materials at sufficiently large laser intensities. The role of this effect on the shape of the craters is examined. This saturation effect is demonstrated to be a consequence of the interplay between the ionization and the light absorption processes. © *2005 Society of Photo-Optical Instrumentation Engineers.* [DOI: 10.1117/1.1904591]

Subject terms: femtosecond; laser ablation; modeling; metals; dielectric materials; material processing.

Paper SS040534 received Aug. 9, 2004; revised manuscript received Nov. 23, 2004; accepted for publication Dec. 22, 2004; published online May 10, 2005.

## 1 Introduction

Recently developed and commercialized femtosecond laser systems have found several industrial and medical applications. In fact, the ultrashort pulse duration provides unique possibilities for very precise treatment/machining of many materials including transparent dielectrics. Among the technologies of particular interest are the microfabrication of polymeric materials and the laser treatment of biological tissues. In addition, spectacular advances in such fields as nanotechnology and microelectronics require the development of smaller and smaller microstructures from semiconductors and metals. This is why many laboratories are now equipped with femtosecond laser facilities and have already reported a number of promising results. For instance, the possibilities of subwavelength structuring of various materials were demonstrated.[1–3]

Despite the demonstrations of the high industrial potential of ultrashort laser pulses, fundamental mechanisms of the interactions of these pulses with different materials are still under discussion. A better understanding of the physical phenomena involved is required to facilitate the further development of new laser technologies. Therefore, in addition to the experimental work, numerous theoretical efforts are aimed at the explanation of such results as subwavelength material structuring and the reduction of thermal damage. A number of theoretical and numerical studies were already undertaken focusing on the investigation of the intrinsic mechanisms of ultrashort laser-matter interactions. Part of these studies were based on the well-known two-temperature model, which assumes a thermodynamic equilibrium inside both electron and lattice/ion subsystems and describes the energy exchange between them during the relaxation time.[4] A more rigorous kinetic approach based on solutions of the Boltzmann equation was also employed in several studies.[5,6] This approach accounts for the possible absence of equilibrium inside the laser-excited electron subsystem. For dielectric materials, the multiphoton and avalanche ionization processes were included in the models. A hydrodynamic (or, fluid) modeling was also performed by several researchers to describe the ultrashort laser ablation and the plasma plume formation.[7] The hydrodynamic approach enables a large-scale description and is of particular interest in the engineering contest.

The numerous investigations provided rich scientific information about femtosecond interactions. A number of issues are, however, still puzzling. For instance, a dramatic change in the quality of the laser treatment with laser fluence is commonly observed in the experiments with femtosecond pulses and is still unclear.[3] These changes were reported in experiments with both dielectric materials and metals. In addition, a drastic difference in the ablation process is found in different metals, which is correlated with the different strength of the electron-lattice/ions coupling.[3] In particular, rather unusual structures were produced in metals with weaker electron-ion ($e$-$i$) coupling parameter (i.e., gold). The conditions of the appearance of these structures are, however, still unclear. The understanding of these effects is not triggered by recent laser plasma characterizations experiments showing surprisingly that both plume temperatures and kinetic energies of plasma species depend only slightly on the fluence in metal target ablation.[8]

0091-3286/2005/$22.00 © 2005 SPIE

In what follows, we present numerical results obtained in the modeling of femtosecond interactions with both metallic and dielectric materials. The main objective is to shed some light on the modifications of the ablation regime with laser fluence in several materials. The models accurately take into account the temperature dependencies of such parameters as the absorption coefficient, the electron heat conductivity, and, particularly, the electron-lattice/ion coupling parameter. The effects of these dependencies on ablation are demonstrated.

## 2 Femtosecond Laser Ablation of Metals

In this section, we present the calculation results obtained in the modeling of laser ablation for two metals with different electron-ion coupling strengths. First, the numerical model is presented. The calculation results for aluminum, a metal with a relatively strong electron-ion coupling and well-known material properties are then presented. Next, we discuss several numerical results obtained for gold, a metal with a much weaker electron-ion coupling.

### 2.1 *Modeling Details*

The femtosecond laser ablation of metals is described by a 1-D one-fluid two-temperature hydrodynamic model.[9] We solve the following system of Lagrange equations:

$$\frac{\partial u}{\partial t}+\frac{\partial(p_e+p_i+q)}{\partial m}=0, \tag{1}$$

$$\frac{\partial v}{\partial t}-\frac{\partial u}{\partial m}=0, \tag{2}$$

$$\frac{\partial \epsilon_e}{\partial t}+p_e\frac{\partial u}{\partial m}=-\frac{\partial H_e}{\partial m}+\frac{\partial S_L}{\partial m}-\gamma(T_e-T_i), \tag{3}$$

$$\frac{\partial \epsilon_i}{\partial t}+p_i\frac{\partial u}{\partial m}=\gamma(T_e-T_i), \tag{4}$$

where $m$, $u$, $v$, $p_{e,i}$, and $\epsilon_{e,i}$ are the Lagrangian mass coordinate, the fluid velocity, the specific volume, the pressure, and the internal energy of the electrons and ions, respectively. Here, $\partial S_L/\partial m$ denotes the absorbed laser energy per mass and time, and $H_e$ is the electron heat flow. The coefficient $\gamma=g/\rho$ determines the electron-ion coupling; $\rho=1/v$ is the fluid density; $g=C/\tau_i$, where $C$ is the heat capacity of the metal lattice; $\tau_i$ is the time required to heat the ions (typically from 1 to 20 ps); and $q$ is the artificial viscosity term that helps to maintain the numerical stability of the calculations. To complete the Lagrange system [Eqs. (1) to (4)], the following conditions are used:

$$\frac{\partial z}{\partial t}(t,m)=u(t,m), \tag{5}$$

$$\frac{\partial z(0,m)}{\partial m}=u(0,m)=0, \tag{6}$$

$$v(0,m)=\frac{1}{\rho_0}, \tag{7}$$

where $z$ is the space coordinate, and $\rho_0$ is the density of the metal target at the room temperature. The metal target is located at $z\leqslant 0$ and $z=0$ is the initial target surface. Laser light absorption is calculated by the solution of the Helmholtz equation by the matrix method together with the modeling of the material motion. For the calculation of material properties, a set of models is organized in the equation of state (EOS), which was tested in ablation experiments. For the electron conductivity, we used the model of Lee and More,[10] which provides transport coefficients, including both electrical conductivity and thermal conductivity. In this model, the transport coefficients are obtained from the solution of the Boltzmann equation in the relaxation time approximation. Different equations are used for the relaxation time in plasma, solid, and liquid phases. For the plasma phase, the electron-ion collision rate is obtained from a Coulomb cross section with appropriate cutoff parameters. For solid and liquid phases, the electron mean free path is obtained from the Bloch-Grüneisen theory using the melting formula derived from Thomas-Fermi theory. More details can be found in Refs. 9 and 11.

Calculations are performed for a Gaussian laser pulse with a 100-fs pulse width at a wavelength of 800 nm. The validity range of the hydrodynamic Lagrangian model is determined mainly by the properties of the EOS and the assumption of local thermodynamic equilibrium. The modeling results, such as ablation depth and plume velocities, are found to agree with metal ablation experiments for laser fluences from 0.2 to 20 J/cm$^2$.

### 2.2 *Calculation Results for Aluminum*

Upon the absorption of femtosecond laser radiation by free electrons, the electron heat diffusion begins in the metal target, which is located at $z\leqslant 0$ ($z=0$ is the initial target surface). The electron heat wave is accompanied by the energy exchange with the lattice/ions and by the buildup and propagation of a hydrodynamic pressure wave. Here, two regimes of laser interactions with the aluminum target can be distinguished:

1. *Laser fluence is small* (here, $0.2<F<1$ J/cm$^2$). In this case, the matter is transferred to plasma in the vicinity of the initial surface position. This transformation can be seen in the target density and velocity curves in Fig. 1(a). In addition, the region of the electron-ion equilibrium is short. Even at $t=8$ ps, the electron and ion temperatures are different everywhere except for a small region [Fig. 1(a)]. This difference means that only a fraction of the electron energy has been transferred into the ion subsystem. The energy fraction increases with the electron temperature (or, with fluence).
2. *Laser fluence is large* (here, $F\geqslant 1$ J/cm$^2$). In this case, at a certain delay after the beginning of the laser pulse, a shock wave (SW) is formed, leading to the discontinuities in the density and velocity curves shown in Fig. 1(b). This happens when the depth of the pressure wave propagation $z_h(t)$

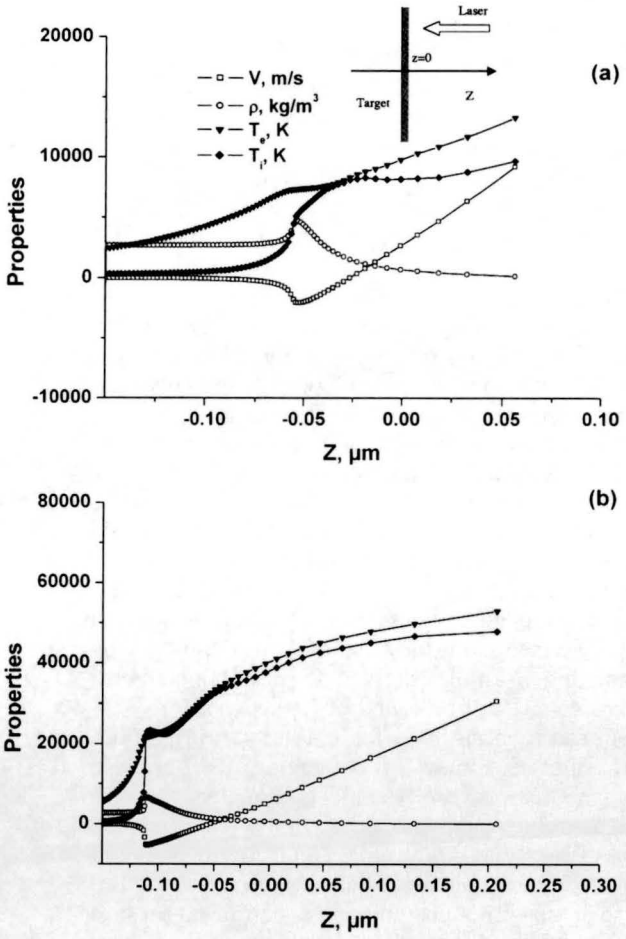


**Fig. 1** Velocity, density, and electron and lattice/ions temperatures calculated $t=8$ ps after the beginning of the laser pulse for aluminum ablation. Here, the pulse wavelength is 800 nm and temporal width is 100 fs. Laser fluence is (a) $F=0.4$ J/cm$^2$ and (b) $F=4$ J/cm$^2$.

$\sim\int_0^t c_s(z,t^*)\mathrm{d}t^*$, where $c_s$ is the speed of sound, becomes comparable with the depth of the heat wave propagation.[12] The region of the $e$-$i$ equilibrium is located behind the SW. In this region, the matter is transformed into rapidly expanding plasma. As late as 8 ps after the laser pulse, however, the electron temperature is still higher than that of lattice/ions beyond the region of $e$-$i$ equilibrium (both deeper in the bulk and in the plasma front).

The two fluence regimes can be also distinguished in Fig. 2, which shows the speed of the electron heat wave propagation as a function of laser fluence. The slope of the dependency changes at $F=1$ J/cm$^2$. Therefore, one can correlate the change in velocity of the heat wave propagation with the appearance of the second ablation regime. Note, in addition, that in most previous numerical studies, only large fluences were used.

The calculation results explain the experimentally observed fluence dependency of the ablation rate. The change in the ablation depth versus fluence dependency was previously attributed to the fact that the optical penetration depth exceeds the heat propagation depth at small fluences.[13] In

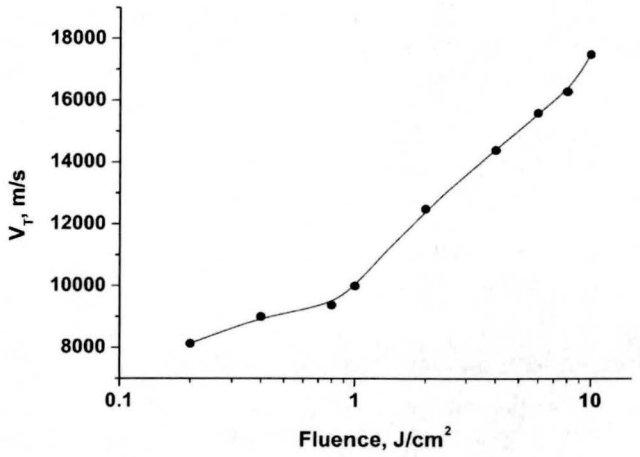


**Fig. 2** Propagation velocity of the electron temperature wave as a function of laser fluence calculated for aluminum ablation at 800 nm and a 100-fs laser pulse.

metals, however, practically always the heated depth is given by the heat diffusion rather than by the skin depth.[12] The modeling results clearly demonstrate that the ablation depth is determined by the temperature-dependent electronic heat conduction. The latter changes sharply with electron temperature and with the matter transformation into plasma. At small fluence, the $e$-$i$ heat transfer is dominated by the electron-phonon interactions, whereas the $e$-$i$ collisions prevail at larger fluences. In addition, the electron heat transport is accompanied by the $e$-$i$ energy exchange, which results in the cooling of the electrons that can also modify the electron heat diffusion.[14]

### 2.3 *Calculation Results for Gold*

Femtosecond laser ablation of metals depends strongly on the strength of the $e$-$i$ coupling.[3,15] In particular, a rather unexpected ablation behavior was observed in metals with a weak $e$-$i$ coupling parameter.[3] To better understand the physical processes taking place in such metallic materials, we performed a series of calculations for gold (Fig. 3). Unlike the results obtained for aluminum, here no $e$-$i$ equilibrium zone is observed as late as at $t=12$ ps even at fluence as large as 20 J/cm$^2$ (the largest in our calculations). Apparently, the weak $e$-$i$ coupling slows down the $e$-$i$ energy exchange and accounts for the difference between $T_e$ and $T_i$. Another consequence of the weak $e$-$i$ coupling is that the electron cooling due to the $e$-$i$ energy exchange is small and it does not affect the electron heat diffusion.

For gold, the ablation process is different at $F=3$ and 20 J/cm$^2$. At the smaller laser fluence, the plasma is formed only near the laser-irradiated surface. At the larger $F$, the plasma transition occurs deeper in the heated material. To understand these regimes, we note that at small $F$ only a small fraction of the electron energy is transferred to the lattice/ions. In addition, both the heat absorption and the $e$-$i$ transfer is apparently more effective near the surface, and the electron heat diffusion is small. At the larger laser fluence, the energy transfer occurs in volume, leading to a rapid overheating and explosive expansion of the material.[16]

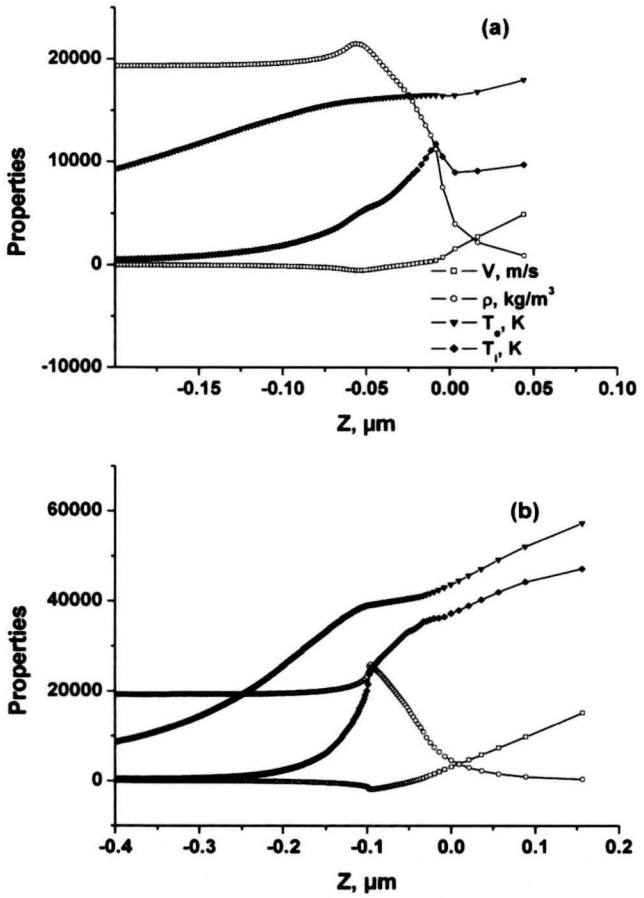


**Fig. 3** Calculated velocity, density, and electron and lattice/ions temperatures obtained at $t=12$ ps after the beginning of the laser pulse for gold. Here, laser pulse wavelength is 800 nm and duration is 100 fs. Laser fluence is (a) $F=3$ J/cm$^2$ and (b) $F=20$ J/cm$^2$.

## 3 Femtosecond Laser Interactions with Dielectric Materials

In this section, we present numerical results obtained for dielectric materials. The details of the modeling of femtosecond laser interaction with dielectric materials are first discussed. The validity range of the model is determined by a comparison of the calculated ablation thresholds with the experimental values available in the literature. The ablation depths obtained in the 1-D modeling are then shown. Finally, the results of the calculations in two dimensions are described.

### 3.1 *Modeling of Material Ionization and Laser Light Absorption*

For the radiation absorption, free carriers should be first created by the ionization of the dielectric materials. Because the bandgap is typically too wide in these materials for the one-photon ionization, so multiphoton ionization creates conduction band electrons. This process may be accompanied by the formation of self-trapped excitons, by the absorption on defects, and by electron impact (avalanche) ionization. The advantage of the application of femtosecond pulses for laser treatment of the transparent (dielectric) materials is that the radiation intensity is sufficiently large for the multiphoton ionization to occur. In addition, avalanche ionization also contributes in the increase of the electron density.[5] To calculate the laser absorption, the following equations are solved:[17–19]

**Table 1** Energy gap, number $n$ of photons implied in the multiphoton ionization, and number density of the valence band electrons $n_V$ for $Al_2O_3$ and for MgO.

| Solid | Energy Gap (eV) | $n$ | $1.57n$ (eV) | $n_v$ (cm$^{-3}$) |
|---|---|---|---|---|
| $Al_2O_3$ | 8.8 | 6 | 9.42 | $1.4\times10^{23}$ |
| MgO | 7.7 | 5 | 7.85 | $10^{23}$ |

$$\frac{\partial n_e(t,r,z)}{\partial t}=(n_V-n_e)\frac{\sigma_n}{(\hbar\omega)^n}I^n+\gamma(I)n_e\frac{n_V-n_e}{n_V}, \tag{8}$$

$$\frac{\partial I(t,r,z)}{\partial z}=-n\hbar\omega(n_V-n_e)\frac{\sigma_n}{(\hbar\omega)^n}I^n-\alpha(n_e)I, \tag{9}$$

with the initial and boundary conditions

$$n_e(t=0,r,z,)=0 \quad \text{for } r\geq 0,\ z\geq 0; \tag{10}$$

$$I(t,r,z=0)=I_0\exp\left[-4\ln 2\left(\frac{t^2}{\tau^2}+\frac{r^2}{r_0^2}\right)\right][1-R(t,r)] \quad \text{for } t\geq 0,\ r\geq 0, \tag{11}$$

where $\tau$ is the pulse width, $r_0$ is the laser spot radius, and $R$ is the reflectivity. Here, the target is located at $z\geq 0$; $r=0$ is the center of the laser spot; $z=0$ is the initial target surface, and the laser beam comes from $z=0$; $n_e$ is the number density of the conduction band electrons; $I$ is the laser intensity; $n_V$ is the number density of valence band electrons in the nonexcited dielectric, $(n_V-n_e)$ is therefore the density of valence electrons for laser excited dielectric; $\sigma_n$ is the cross section of multiphoton ionization, where $n$ is the minimum number of photons to traverse the energy gap; $\gamma(I)$ is the avalanche constant; $\omega$ is the laser frequency; and $\alpha(n_e)$ is the absorption coefficient by conduction band electrons given by the modified Drude model.[19] In Eq. (8), we disregarded electron losses due to self-trapped exciton formation and recombination processes. This is justified for the materials we used, in which these processes occur at a time scale much longer than the pulse width. Electron thermoemission and thermal conductivity are also neglected, and the model is applicable only when the optical penetration depth is larger than the depth of the heat propagation. The calculations are therefore performed for laser pulses shorter than 1 ps and only until the end of the laser pulse. This implies that the ablation takes place rapidly, as discussed hereafter.

### 3.2 *Comparison of the Calculation Results with Experiments*

To evaluate the ablation depth and the ablated crater shape we use the following ablation criteria: we assume that the

**Table 2** Multiphoton ionization cross section $\sigma_n$ and collision frequency $\nu_c$ for MgO.

| Pulse Duration (fs) | $\sigma_5$ ($cm^{10} s^4$) | $\nu_c$ ($fs^{-1}$) |
|---|---|---|
| 80 | $7 \times 10^{-150}$ | 0.77 |
| 730 | $2.5 \times 10^{-149}$ | 0.77 |
| 1300 | $2.5 \times 10^{-149}$ | 0.77 |

material is ablated if at the end of the laser pulse the electron density reaches at least the critical electron density

$$n_c = \frac{\omega^2 m_e \epsilon_0}{e^2}, \tag{12}$$

where $m_e$ is the electron mass, $e$ is the electron charge, and $\epsilon_0$ is the vacuum permitivity. In the case of dielectric materials, the ablation process more probably proceeds via a combination of a Coulomb explosion with a nonequilibrium thermal or mechanical ablation that occur before the electron heat diffusion becomes considerable.[20]

We calculated the ablation threshold for two dielectric materials $Al_2O_3$ and MgO with varied laser pulse durations. To obtain a better agreement with the experiments the avalanche term was neglected in these calculations. This simplification is justified by the recent full kinetic calculations[21] that proved a much smaller (~10 times) contribution of the impact ionization process with respect to the one obtained from a common estimation given by Eq. (8). The calculation results in the center of the laser spot ($r=0$) are compared with the experimental findings.[19] Table 1 gives the energy gap, the number $n$ of photons implied in the multiphoton ionization, and the number density of the valence band electrons $n_V$ for $Al_2O_3$ and for MgO. Note here that a laser wavelength of 790 nm corresponds to the photon energy of 1.57 eV. To calculate the ablation threshold for these materials, we used experimentally measured parameters (the multiphoton ionization cross section $\sigma_n$ and the collision frequency $\upsilon_c$). Tables 2 and 3 summarize these parameters for MgO and $Al_2O_3$ respectively. Tables 4 and 5 show the comparison of the calculated and experimental values of the ablation threshold.

One can see that for laser pulses shorter than about 1000 fs, the calculated ablation thresholds agree with the experimental ones. However, for pulses longer than or equal to 1300 fs for MgO and 1200 fs for $Al_2O_3$, the calculated differ considerably from the measured thresholds. This result may be attributed to the fact that when laser pulse is longer than 1000 fs, several nonconsidered physical processes start playing a role, such as, for example, electron heat diffusion. It is also possible that the contribution of avalanche ionization becomes considerable for longer laser pulses.

**Table 3** Multiphoton ionization cross section $\sigma_n$ and collision frequency $\nu_c$ for $Al_2O_3$.

| Pulse Duration (fs) | $\sigma_6$ ($cm^{12} s^5$) | $\nu_c$ ($fs^{-1}$) |
|---|---|---|
| 80 | $3 \times 10^{-182}$ | 0.83 |
| 790 | $6 \times 10^{-181}$ | 0.83 |
| 1200 | $10^{-181}$ | 1 |

**Table 4** Calculated and experimental values of the ablation threshold for MgO.

| Pulse Duration $\tau$ (fs) | Experimental Ablation Threshold ($W/cm^2$) | Calculated Ablation Threshold ($W/cm^2$) |
|---|---|---|
| 80 | $3.90 \times 10^{13}$ | $3.81 \times 10^{13}$ |
| 730 | $1.83 \times 10^{13}$ | $1.90 \times 10^{13}$ |
| 1300 | $1.27 \times 10^{13}$ | $1.69 \times 10^{13}$ |

The comparison performed demonstrates the validity of the calculations in the certain range of laser intensities and pulse durations (laser pulse shorter or about 1 ps). We can, therefore, use the model for the investigation of the femtosecond interactions with dielectric materials.

### 3.3 *Calculation Results for the Ablation Depth: Saturation of the Absorption at Large Fluences*

First, the ablation depth as a function of the laser fluence is investigated (Fig. 4). In our calculations, the ablation depth corresponds to the maximum $z$, where the conduction band electron density overcomes the critical density given by Eq. (10). A very well defined threshold fluence, at which the ablation depth starts to rise abruptly, is clearly observed. This fluence is required to excite enough electrons to the conduction band. The conduction band electron density increases with fluence until a certain value $n^*(z)$ and then saturates. The saturation density $n^*(z)$ decreases with the depth, so that only in the layer of several hundred nanometers the conduction band electron density rises enough for the ablation. Beyond this thin layer, the electron density is nearly constant with fluence and remains too small for the ablation.

The saturation effect is visualized in Fig. 5, which presents the density profiles of the conduction band electrons for several laser intensities. The profiles tend to squeeze toward the surface with fluence. As a result, the intersection depth of the curves with $n=n_c$ first increases with laser intensity and then does not change considerably. A similar trend is observed in the profiles of the absorbed energy (Fig. 6). This effect may be understood from the facts that with the rise in the conduction band electron density both

**Table 5** Calculated and experimental values of the ablation threshold for $Al_2O_3$.

| Pulse Duration $\tau$ (fs) | Experimental Ablation Threshold ($W/cm^2$) | Calculated Ablation Threshold ($W/cm^2$) |
|---|---|---|
| 80 | $4.60 \times 10^{13}$ | $3.95 \times 10^{13}$ |
| 790 | $1.89 \times 10^{13}$ | $1.64 \times 10^{13}$ |
| 1200 | $1.20 \times 10^{13}$ | $2.06 \times 10^{13}$ |

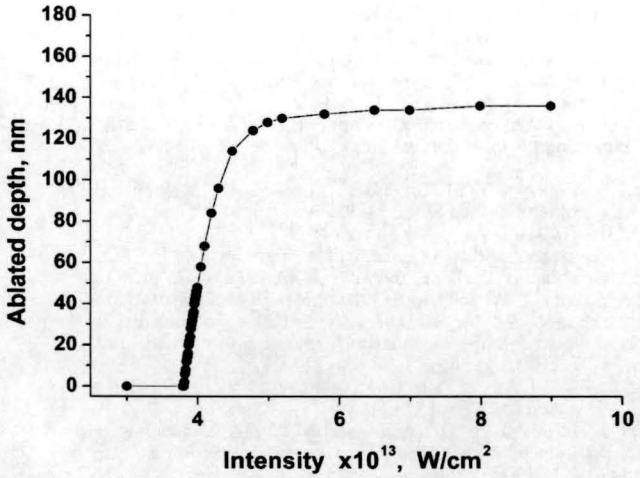


**Fig. 4** Ablated depth versus peak laser intensity for MgO. Here, the pulse duration is 80 fs, the wavelength is 790 nm, and the calculated critical density is $n_c = 1.785 \times 10^{21}$ cm$^{-3}$.

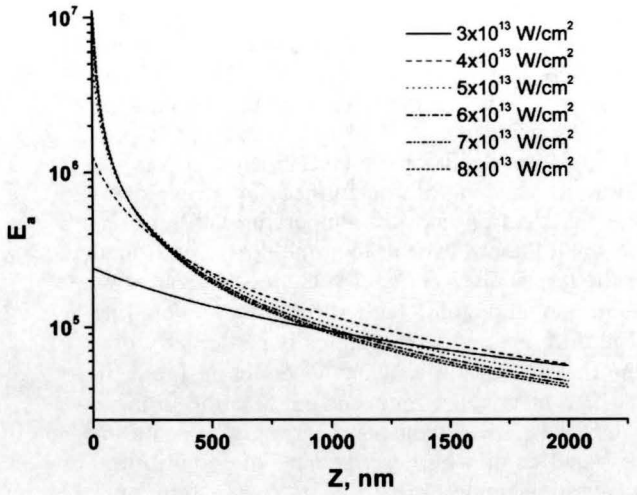


**Fig. 6** The fraction $E_a(z)$ of the absorbed energy as a function of depth for MgO ablation calculated for different peak laser intensities $I_0$. Here, the pulse duration is 80 fs and wavelength is 790 nm.

the light absorption and reflection grow up considerably. In what follows, the effect of the saturation on the crater shape will be shown.

### 3.4 *Two-Dimensional Crater Shape in Dielectric Materials*

By solving the Eqs. (8) to (11) for a series of points $r \geq 0$ we obtain 2-D crater shapes. This procedure is particularly simplified if the heat diffusion is negligible, which is the case in the calculations until the end of the laser pulse. The calculated evolution of the crater shape with laser fluence is displayed in Fig. 7. One can see that at small fluences, the ablated craters look similar to a Gaussian profile. With an increase in laser intensity, however, the craters become more and more bottom-plate. A similar change in the crater shape was reported in the ablation experiments for semiconductors[22] as well as in the recent calculations.[23] This change can be attributed to the effect of the saturation of laser light absorption at a certain depth (Figs. 4 to 6). In fact, because the radial shape of the laser beam intensity is Gaussian, the ablation depth saturation is more pronounced near the crater center. As a result, at a sufficiently large laser fluence, the crater shape approaches the one that is obtained with a top-hat pulse. In other words, Gaussian pulses may, under certain conditions, produce craters in dielectric materials similar to the those obtained with top-hat pulses. The laser intensity required for this effect is limited by the conditions of the appearance of thermal effects (such as melting, for example), which are not considered in the presented calculations for dielectrics.

## 4 Summary and Conclusions

We carried out a numerical modeling of the laser ablation of both metallic and dielectric targets by ultrashort laser pulses. Particular attention focused on the investigation of the fluence dependencies of the ablation regimes. For this, a series of calculations were performed with temperature-dependent material properties, such as the absorption coefficient, electron heat conductivity, the electron-ion coupling parameter, etc. These calculations demonstrated a crucial role that these dependencies play in the ablation process.

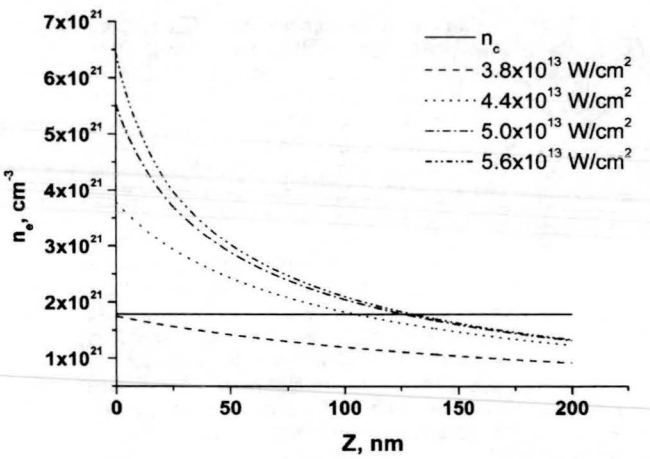


**Fig. 5** Number density of the conduction band electrons versus depth for several peak laser intensities $I_0$ obtained for MgO ablation. The line $n = n_c$ is also shown. Here, the pulse duration is 80 fs and the wavelength is 790 nm.

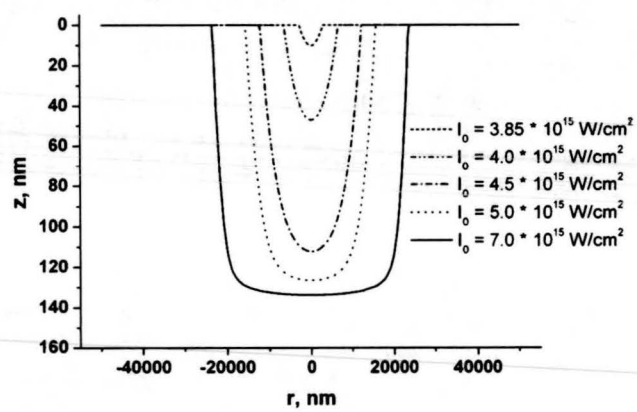


**Fig. 7** Ablated crater shapes calculated for MgO for the pulse duration of 80 fs, a wavelength of 790 nm, and for different peak laser intensities $I_0$.

The calculations performed for metals, where conduction band electrons are already present, show that the electron heat conduction changes drastically with laser fluence. Both the change in the electron heat conduction and the phase transitions in the target lead to a nonlinear dependency of the ablation depth versus laser fluence.

In addition, the calculations performed for metals demonstrate that the electron and ion temperatures differ considerably at small fluence even at the time delays of around 10 ps after the laser pulse. These effects are shown for two metals, aluminum and gold, with different $e$-$i$ coupling strength. The difference in temperatures is particularly dramatic in the metal with the weaker $e$-$i$ coupling (gold, in our case), which means that femtosecond ablation in these materials should be considered as a strongly nonequilibrium process and cannot be described by the equilibrium thermal evaporation model. In particular, only a thin layer of the material will be heated to the sufficient temperatures at small fluence, leading to the surface effects such as deformations and instabilities.

In dielectric materials, the creation of free carriers by ionization and their subsequent heating by laser light absorption are both temperature-dependent processes. With laser fluence, the rise in the electron density above the critical density leads to the more and more enhanced absorption near the surface. These processes bring about the saturation in the ablation depth at sufficiently large laser fluences. The saturation significantly affects the shape of the laser-treated craters. This effect is particularly pronounced when laser fluence is in a certain range, so that thermal effects can be negligible. Knowledge of the ablation depth versus fluence dependency at laser intensities below the one required for saturation can help one to predict a 2-D crater shape for a given radial distribution of the laser beam.

In conclusion, the numerical results showed several nonlinear fluence effects in the femtosecond ablation of both metals and dielectrics. The ablation modeling performed with temperature-dependent calculation parameters, such as $e$-$i$ collision frequency and electron heat conduction, clearly demonstrated the crucial role of these physical phenomena in ultrafast laser interactions. In addition, a strong fluence dependency of the ablation depth was explained for dielectric materials. The results obtained are of importance for the development of numerous applications of femtosecond laser systems, such as micromachining, microstructuring, medical applications, surface marking, etc.

## Acknowledgments

We are grateful to François Vidal for supplying us with important parts of the hydrodynamic ablation code. We would like to acknowledge the IDRIS and the CINES of France for computer support.

## References

1. P. P. Pronko, S. K. Dutta, J. Squier, J. V. Rudd, D. Du, and G. Mourou, "Machining of sub-micron holes using a femtosecond laser at 800 nm," *Opt. Commun.* **114**, 106 (1995).
2. C. Momma, B. N. Chichkov, S. Nolte, F. von Alvensleben, A. Tünnerman, and H. Welling, "Short-pulse laser ablation of solid targets," *Opt. Commun.* **129**, 134 (1996).
3. F. Korte, J. Serbin, J. Koch, A. Egbert, C. Fallnich, A. Ostendorf, and B. N. Chichkov, "Towards nanostructuring with femtosecond laser pulses," *Appl. Phys. A: Solids Surf.* **77**, 229–235 (2003).
4. S. I. Anisimov, A. M. Bonch-Bruevich, M. A. El'yashevich, Ya. A. Imas, N. A. Pavlenko, and G. S. Romanov, "The action of powerful light fluxes on metals," *Sov. Phys. Tech. Phys.* **11**, 945 (1967).
5. B. Rethfeld, K. Sokolowski-Tinten, D. von der Linde, and S. I. Anisimov, "Ultrafast thermal melting of laser-excited solids by homogeneous nucleation," *Phys. Rev. B* **65**, (2002).
6. G. Colonna, A. Casavola, and M. Capitelli, "Modeling of LIBS plasma expansion," *Spectrochim. Acta, Part B* **56**(6), 567–586 (2001).
7. Y. Y. Tsui, J. Santiago, Y. M. Li, and R. Fedosejevs, "Melting and damage of aluminum surface by 80 ps KrF laser pulses," *Opt. Commun.* **111**, 360 (1994).
8. D. Grojo, J. Hermann, and A. Perrone, "Plasma analysis during femtosecond laser ablation of Ti, Zr, and Hf," *J. Appl. Phys.* (in press).
9. F. Vidal, S. Laville, T. W. Johnston, O. Barthelemy, M. Chaker, B. Le Drogoff, J. Margot, and M. Sabsabi, "Numerical simulation of ultrashort laser pulse ablation and plasma expansion in ambient air," *Spectrochim. Acta, Part B* **56**(6), 973–986 (2001).
10. Y. T. Lee and R. M. More, "Electron conductivity model for dense plasmas," *Phys. Fluids* **27**(5), 1273 (1984).
11. T. E. Itina, J. Hermann, Ph. Delaporte, and M. Sentis, "Modeling of metal ablation induced by ultrashort laser pulses," *Thin Solid Films* **453–454**, 513–517 (2004).
12. K. Eidmann, J. Meyer-ter-Vehn, T. Schlegel, and S. Hüller, "Hydrodynamic simulation of subpicosecond laser interaction with solid-density matter," *Phys. Rev. E* **62**(1), 1202 (2000).
13. C. Momma, S. Nolte, B. Chichkov, F. v. Albensleben, and A. Tünnermann, "Precise laser ablation with ultrashort pulses," *Appl. Surf. Sci.* **109**, 15 (1997).
14. S. D. Brorson, J. G. Fujimoto, and E. P. Ippen, "Femtosecond electronic heat-transport dynamics in thin gold films," *Phys. Rev. Lett.* **59**(17), 1962–1965 (1987).
15. D. S. Ivanov and L. V. Zhigilei, "Combined atomistic-continuum modeling of short-pulse laser melting and disintegration of metal films," *Phys. Rev. B* **68**, (2003).
16. B. J. Garrison, T. E. Itina, and L. V. Zhigilei, "Limit of overheating and threshold behavior in laser ablation," *Phys. Rev. E* **68**, (2003).
17. B. C. Stuart, M. D. Feit, S. Herman, A. M. Rubenchik, B. W. Shore, and M. D. Perry, "Nanosecond-to-femtosecond laser-induced breakdown in dielectrics," *Phys. Rev. B* **53**, 1749 (1996).
18. S. S. Mao, F. Quéré, S. Guizard, X. Mao, R. E. Russo, G. Petite, and P. Martin, "Dynamics of femtosecond laser interactions with dielectrics," *Appl. Phys. A: Solids Surf.* **79** , 1695-1709 (2004).
19. F. Quéré, "Study of the electronic excitation mechanisms involved in laser-induced breakdown of dielectrics," PhD Thesis, Paris VI University (2000).
20. D. Ashkenasi, G. Muller, A. Rosenfeld, R. Stoian, I. V. Hertel, N. M. Bulgakova, and E. E. B. Campbell, "Fundamentals and advantages of ultrafast micro-structuring of transparent materials," *Appl. Phys. A: Solids Surf.* **77**, 223 (2003).
21. B. Rethfeld, "Unified model for free-electron avalanche in laser-irradiated dielectrics," *Phys. Rev. Lett.* **92**(18), (2004).
22. A. S. Zakharov, M. V. Volkov, I. P. Gurov, V. V. Temnov, K. Sokolovski-Tinten, and D. von der Linde, "Interferometric diagnostics of ablation craters formed by femtosecond laser pulses," *J. Opt. Technol.* **69**, 478 (2002).
23. L. Jiang and H. L. Tsai, "Prediction of crater shape in femtosecond ablation of dielectrics," *J. Phys. D* **37**, 1492 (2004).

**Tatiana E. Itina** received her MSc degree in applied mathematics and physics from the Moscow Institute of Physics and Technology, Russia, in 1994, with a research subject on the development of statistical simulation methods for the propagation of laser radiation in diffusive and scattering media. In 1999, she received her PhD degree in physics from The University of Aix-Marseilles, France, with a thesis focused on the Monte Carlo simulation of pulsed laser ablation. From 2000 to 2001, Dr. Itina was a postdoctoral research associate with the Pennsylvania State University, USA, working on the molecular dynamics simulation of matrix-assisted laser desorption ionization (MALDI). In 2002, Dr. Itina joined the French National Center for Scientific Research (CNRS). She is currently a research staff member with the Laboratory of Lasers, Plasma and Photonic Processing in Marseilles, where she is responsible for the modeling of laser-matter interactions. Her research interests include both microscopic and continuous modeling of laser interactions, the dynamics of plasma plume expansion, the study of microscopic mechanisms of laser ablation, and the synthesis of nanoclusters by laser ablation.

**Mikhail Mamatkulov** received his BSc degree in physics from Joseph Fourier University, Grenoble, France, in 2002 and his MSc degree in materials science from the University of Aix-Marseilles in 2004. During his undergraduate studies he spent 1 year at the University of Montreal, Canada, as an international exchange student. In the framework of his MSc studies Mamatkulov trained first with the Laboratory of Electronics and Information Technology of the French Atomic Energy Commission (CEA/LETI), where he worked on the finite-element modeling of thermomechanical properties of silver thin films. He then worked on the numerical modeling of femtosecond laser interactions with dielectric materials with the Laboratory of Lasers, Plasmas and Photonic Processing. He is currently preparing for his PhD degree in numerical materials science at the Laboratory of Physics and Electronic Spectroscopy, Mulhouse, France.

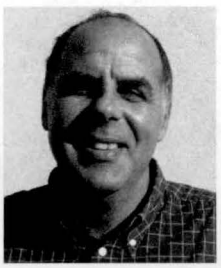

**Marc Sentis** received his engineer diploma in energetics from the Ecole Nationale Superieure des Arts et Metiers, Paris, in 1980 and his PhD and "Doctorat d'Etat" degrees in applied physics from the Aix-Marseille University in 1982 and 1988, respectively. In 1983, Dr. Sentis joined the French National Center for Scientific Research (CNRS). He was a staff member at the Institute of Fluid Mechanics of Marseilles from 1983 to 1994 and then was with the Institute of the Research on Non-Equilibrium Phenomena. Since 2000 he has directed the Laboratory of Lasers, Plasmas and Photonic Processing (LP3) in Marseilles, France. His current interests and research include ultrafast laser physic, excimer lasers, gas discharges, and laser ablation in the femtosend and nanosecond regimes.